Prior cocaine use disrupts identification of hidden states by single units and neural ensembles in orbitofrontal cortex

Wenhui Zong [1*], Lauren E. Mueller[1], Zhewei Zhang [1], Jingfeng Zhou [2*t], and Geoffrey Schoenbaum [1*t]

[1] National Institute on Drug Abuse, Intramural Research Program, Baltimore MD 21224
[2] State Key Laboratory of Cognitive Neuroscience and Learning, Beijing Normal University & Chinese Institute of Brain Research, Beijing 100875, China

* Corresponding authors
t senior authors

Abstract

The orbitofrontal cortex (OFC) is critical to identifying task structure and to generalizing appropriately across task states with similar underlying or hidden causes. This capability is at the heart of OFC's proposed role in a network responsible for cognitive mapping, and its loss can explain many deficits associated with OFC damage or inactivation. Substance use disorder is defined by behaviors that share much in common with these deficits, such as an inability to modify learned behaviors in the face of new information about undesired consequences. One explanation for this similarity would be if addictive drugs impacted the ability of OFC to recognize underlying similarities – hidden states – that allow information learned in one setting to be used in another. To explore this possibility, we trained rats to self-administer cocaine and then recorded single unit activity in lateral OFC as these rats performed in an odor sequence task consisting of unique and shared positions. In well-trained controls, we observed chance decoding of sequence at shared positions and near chance decoding even at unique positions, reflecting the irrelevance of distinguishing these positions in the task. By contrast, in cocaine-experienced rats, decoding remained significantly elevated, particularly at the positions that had superficial sensory differences that were collapsed in controls across learning. These neural differences were accompanied by increases in behavioral variability at these positions. A tensor component analysis showed that this effect of reduced generalization after cocaine use also extended across positions in the sequences. These results show that prior cocaine use disrupts the normal identification of hidden states by OFC.

Introduction

The orbitofrontal cortex (OFC) is essential for recognizing the underlying structure of tasks and for generalizing across contexts that share hidden or latent causes[1-6] .This capacity allows animals to infer the common features between seemingly different experiences and to adjust behavior accordingly—a process at the core of cognitive mapping[7,8]. When this ability is disrupted, behavior can become overly tied to superficial sensory features, leading to inflexible or maladaptive responses[9]. Such impairments have been linked to OFC lesions or inactivation and may also underlie certain features of substance use disorders, which are characterized by the persistence of maladaptive behaviors despite adverse outcomes. One possible explanation for this behavioral rigidity is that chronic drug exposure compromises the OFC's ability to recognize hidden similarities between situations, thereby disrupting generalization across task states. Combined with pre-existing conditions and other environmental insults in certain individuals, such an effect could lead to the loss of behavioral control that characterizes addiction.

To investigate this possibility, we examined how prior cocaine use affects OFC representations of hidden states in a sequential decision-making task. Rats were trained to self-administer either cocaine or sucrose and were then recorded from the lateral OFC while performing an odor-based sequence task with positions that either shared or differed in sensory cues. This task design allowed us to assess whether OFC neurons appropriately compressed or generalized across positions with different sensory features but identical behavioral relevance—a hallmark of hidden state identification. We hypothesized that cocaine-experienced rats would show preserved discrimination of superficial sensory differences that are normally collapsed during learning, reflecting a failure to identify the underlying task structure that makes such distinctions behaviorally irrelevant. As expected, OFC neurons in controls showed near-chance discrimination between comparable positions (P2 and P3) across sequences, reflecting compression of irrelevant sensory differences, and even at positions with unique sensory cues (P1 and P4), neural discrimination was near chance in most trial epochs. This neural compression reflects the OFC's preference to represent latent task states rather than external features. By contrast, cocaine-experienced rats maintained significantly higher selectivity at both shared and unique positions, failing to compress positions that were behaviorally equivalent. Their behavior also became more variable, suggesting reduced recognition of underlying equivalence across sequences. Tensor component analysis (TCA) showed that this loss of generalization extended beyond specific position pairs: cocaine-experienced rats lacked higher-order components that generalized across all positions, indicating a fundamental alteration in how OFC organizes task representations.

These findings demonstrate that cocaine exposure produces a lasting impairment in the OFC's ability to identify and generalize across hidden states. In well-trained animals, OFC activity normally evolves to encode task-relevant structure while suppressing irrelevant sensory differences, a hallmark of cognitive abstraction. Cocaine disrupted this refinement, reverting OFC coding to a more stimulus-bound state reminiscent of early learning. This failure to generalize may help explain why individuals with substance use disorders struggle to modify behavior in response to changing contingencies. When the OFC cannot link distinct experiences through shared underlying causes, learning about the negative consequences of drug use in one context may fail to influence behavior in another. Similarly, extinction or therapeutic interventions may generalize poorly beyond the treatment setting. Thus, the present results identify a neurophysiological mechanism—loss of OFC-mediated generalization—that may underlie the persistence and context-specificity of drug-seeking behavior, providing a new window into how addictive drugs alter cognitive mapping and flexible decision-making in the brain.

Results

To examine the potential impact of cocaine use on the identification of hidden states by OFC neurons, we used a go, no-go odor discrimination task (Figure 1A). This task, used previously to record in OFC [10], featured 6 odors arranged in two 4-odor sequences, labeled as S1 and S2 (Figure 1B). These sequences had unique odors at the start and end positions (P1 and P4) and shared odors at the two positions in the middle, where the sequences overlapped (P2 and P3). The experiment was conducted over a 4-month period consisting of several phases (Figure 1C). Initially, naive rats underwent a four-week training on the "figure 8" task. In the subsequent week, rats underwent jugular catheterization surgery and were given time to recover. For the following two weeks, rats were trained to self-administer either sucrose (10% wt/vol; n = 3) or cocaine (0.75 mg/kg/infusion; n = 3) (Figure 1D), using procedures similar to those known induce incubation of craving [11]. The subsequent three weeks were dedicated to electrode implantation surgery in OFC and post-surgical recovery. Two additional weeks were then allocated for reminder training on the odor task. Finally, *in vivo* recordings were obtained during the last four weeks while the rats performed the odor task.

During these recording sessions, rats in both groups displayed consistently high levels of discrimination performance across all positions in the odor sequence (Figure 1F). In this study, rats were first trained on the odor sequence task to criterion before undergoing cocaine self-administration. Thus, all animals had already acquired the task thoroughly prior to drug exposure, and the task itself was relatively simple. Nevertheless, we observed several robust and significant differences between the cocaine- and sucrose-trained groups. Differences in trial initiation latencies were observed (Figure 1H), suggesting that the rats in both groups utilized the predictable odor sequence to anticipate the availability of reward not only in the current trial but also in subsequent trials. ANOVAs revealed a variety of small but significant group differences in these measures (Figure 1F-H). In addition to these somewhat idiosyncratic differences, analyses also showed effects in line with the proposal that past cocaine use had affected the rats' ability to ignore external differences between positions across the two sequences. Specifically, the behavior of the rats that had self-administered cocaine was more variable across sequences. This was evident in the distribution of difference scores between positions in each sequence on all three measures, which were larger in the cocaine group than in controls (Figure 1I-J). Thus, even after extensive training, animals with a history of cocaine exposure maintained a stronger behavioral distinction between the same position in the two sequences, in all three behavioral measures.

Prior cocaine use disrupts identification of hidden states across position pairs

During these sessions, we recorded a total of 1,699 units in the lateral OFC of thee rats in the cocaine group and 2,182 units from three rats in the control group (Figure 1E). A cursory examination of single-cell examples (Figure 2 A-D) indicated that prior cocaine use was associated with less uniform neural activity at individual positions across sequences. To investigate this effect, we tested whether cocaine use affected the ability of single units and ensembles in the OFC to discriminate between positions in the task, starting with comparisons between the same positions on sequences S1 and S2. Neuronal selectivity on trials at comparable positions in the two sequences was calculated for each trial epoch, and the results showed that the proportion of selective units was very low—essentially at chance during trials at P2 and P3—before increasing at the end of P3 and into the odor sampling periods of P4 and P1 (Figure 2E, top panel). This pattern reflected compression of positions in the central arm of the figure-8 maze, where the two sequences were

identical, and discrimination of positions on the outer arms of the maze, where the odors differed. Notably, however, even for P4 and P1, most epochs within the trial showed near chance levels of selectivity in controls (Figure 2E, top panel), while neurons recorded in cocaine rats maintained significantly higher levels of selectivity (compared both to controls and chance) at the end of P3 and during most of the epochs in P4 when compared directly between the two groups (Figure 2E, bottom panel and Figure 2F).

To quantify this effect, we conducted a two-way ANOVA on the activity of each neuron at each position in the two sequences, with sequence and position as factors. This analysis revealed disproportionate effects of cocaine on the prevalence of neurons showing a significant interaction between these two factors (Figure 3—figure supplement 2), suggesting increased divergence in neural activity at similar positions across sequences in the cocaine group. This impression was reinforced by a second analysis, in which we correlated the preferred position of each neuron in each epoch across sequences. For this, we first identified position selective neurons independently at each epoch and on each sequence (ANOVA, $p<0.01$). A neuron's preferred position was then taken as the position with the highest firing, and then we calculated a correlation coefficient for each group across all neurons and epochs. As shown in the plot, the Sucrose group exhibited a steeper correlation compared to the Cocaine group. To statistically compare the correlation coefficients, we used Fisher's r-to-z transformation and found a significant difference between the groups (Figure 3—figure supplement 3).

The increase in differential activity across sequences in the cocaine group was also evident in an ensemble decoding analysis (Figure 3A). Decoding accuracy was above chance for most epochs at positions P1 and P4 and at the end of the trial and into the ITI period at P3, and while this was true in both groups, the decoding accuracy was significantly higher in the cocaine group in nearly all epochs. This difference between groups was even more evident when average decoding across epochs at each position was directly compared between the two groups (Figure 3B). Thus, both single unit and ensemble activity in lateral OFC in cocaine-experienced rats compressed meaningful task epochs less than in sucrose-trained controls. Additional analyses examining decoding across all positions within- and across-sequences showed that the Cocaine group exhibited significantly higher decoding accuracy within-sequence and significantly lower decoding accuracy across-sequence, compared to the Sucrose group (Figure 3D-G).

Interestingly the effect of cocaine was similar to the effect of diminished training on the task. This is evident in a comparison to data from OFC in rats in a prior study using the same task [10], in which there was much less training prior to recording (6 weeks of odor task training in total plus 2 weeks of self-administration in this study vs. ~3 weeks of odor task training in the prior study). OFC neurons recorded in these rats revealed preserved decoding relative to the over-trained controls in the current study, decoding that was similar to that in the cocaine rats (Figure 3C). Similar effects of training were also evident in OFC neurons recorded in a more complex odor sequence task, also reported previously recorded in a different set of rats [12], where the preservation of decoding between positions was linked to behavioral relevance (Figure 3—figure supplement 1). Thus, neural activity in OFC evolves during learning, to identify the underlying hidden states that define behavioral relevance. This refinement or its specificity is disrupted by prior cocaine use.

Prior cocaine use disrupts identification of hidden states across all positions

While the planned analyses conducted above show that prior cocaine use was associated with preserved discrimination of incidental information about task positions normally compressed by rats performing this task, they do not address whether this is a general effect or whether it only impacted direct comparison of the position pairs highlighted by the analyses. That is, did neurons in the cocaine-experienced rats maintain information about these positions because of the idiosyncratic features of our task, or is there a general effect of cocaine on the ability of the OFC to register common features and underlying causes. To get at this more general question, we utilized tensor component analysis (TCA) to identify the dominant factors shaping neural activity across units, epochs, and trials in our task. This analysis provides a less constrained, more hypothesis-agnostic approach to our question since it looks for patterns across all of these factors in the design. If cocaine is causing a failure of generalization more broadly, then we would expect loss of power in dimensions across positions and not just within position pairs.

The results for this analysis are shown in Figures 4A-B and Figure 4—figure supplement 1. Neural variance was partitioned into components, one per row. The analysis shown was constrained to 10 components, as this number produced the most consistent and reliable results compared to other choices (Figure 4—figure supplement 2-3); additionally, the features we will highlight for each group were generally consistent within individual rats from each group (Figures S7-8). For each group, the characteristics of each component are visualized by the contributing neuron weight (left), temporal dynamics within a trial (middle), and amplitude of such dynamics across trials organized by positions (right). Thus, to discuss one example, the top row in the control group shows that the first component was broadly distributed across neurons (left panel), expressed most strongly in the later trial epochs (middle panel), and exhibited low amplitude at P1 and P4 and high at P2 and P3 (right panel). Further, it was higher in P3 than P2 and also showed similar patterns across trials within each of these position pairs (right panel).

After aligning these component patterns between groups based on their temporal factors, we observed different patterns in trial amplitudes reflecting differences in positional representations (right columns). In controls, most of the trial factors distinguished between the position pairs (rows 1–3, 6, 7, 8, 10). These factors distinguished rewarded from non-rewarded position pairs, in some cases further distinguishing particular position pairs within each category (rows 2,3,7,8) and/or showing effects of trials (rows 2,3). However, none showed differences between positions or trials inside a pair. This result is consistent with findings in Figure 2 and 3, which showed that both individual units and ensemble responses in control rats collapsed the positions within each pair. However, controls also had three additional factors that appeared to generalize not just across positions inside a pair but rather across all positions (rows 4, 5, 9). These factors were identical across all 8 positions and two (rows 5 and 9) showed identical changes across trials within each position. This indicates a significant tendency in neural activity in OFC to represent commonalities across all 8 positions dynamically across time in a session; this global generalization goes beyond that illustrated in our planned comparisons in Figures 2 and 3.

The trial factor patterns in the cocaine-experienced rats were substantially different; all of the 10 factors distinguished rewarded versus non-rewarded position pairs, and the position-general factors evident in controls (rows 4, 5, 9) were absent from activity in the cocaine rats. This dichotomy is consistent with reduced compression evident in our planned comparisons in Figures 2 and 3 and further points to diminished generalization across task features and a heightened emphasis on differences across positions in the task, which presumably reflects the different values

imparted by the sequences. These general features were robust and interpretable across animals in both the Sucrose and cocaine-exposed groups (Figure 4—figure supplement 4-5). This consistency supports the validity of comparing TCA-derived measures across groups, and consistency across individuals within each group.

To quantify the differences in Figures 4A–B, we used mutual information (MI) to measure the information available in each factor—particularly factors 5 and 9 about position and trial. Consistent with the description above, we found lower MI values for position in controls at these components compared to the cocaine group (Figure 4C) and higher MI at the same components for trial or temporal information (Figure 4D). Moreover, similar results were observed across varying numbers of components, with the significant difference between the two groups remaining consistent regardless of the number of components selected (Figure 4—figure supplement 2-3).

Discussion

These results are consistent with a cocaine-induced disruption of the normal identification of underlying hidden states by OFC [1-6]. Specifically, in the current task, OFC representations normally evolve with training to compress or generalize similar positions in the two sequences, even when external sensory information—the odor cues—differ. Cocaine-experienced rats failed to show this normal compression of irrelevant information, instead discriminating these position pairs at higher rates, similar to encoding observed in rats early in learning. Additionally, this failure to generalize was also evident in a TCA analysis, where factors generalizing across different positions were prominent in control data but entirely absent in data from cocaine-experienced rats.

The loss of this normal function of OFC is relevant to addiction, since it suggests that some addictive drugs, at least the psychostimulants, cause fundamental and long-lasting changes in how prefrontal areas process task-related information. These effects are consistent with prior studies showing changes in OFC function after drug use, particularly for behaviors in which hidden states are particularly critical, such as devaluation and sensory preconditioning or even reversal [13-18]. The current findings extend this work to show a specific effect on generalization or the ability of OFC neurons to collapse trivial external information to encode underlying causes that different situations have in common. A loss of this ability could have wide ranging effects [19], but it might particularly disrupt the mobilization of learning from other settings to counteract or diminish drug-seeking behaviors. For instance, consequences of drug use learnt in separate contexts or situations – for instance at home or in the classroom, during counseling, or even from observing the impact of drug use in the lives of others - would not be as effectively deployed to affect behavior during one's own drug-seeking. Similarly therapeutic approaches designed to extinguish drug-seeking would also generalize more poorly outside of the clinical setting. The current data provides a neurophysiological correlate, induced by drug-use, that could underlie such well-known effects.

Figure Captions

Figure 1. Figure 8 odor sequence task, cocaine self-administration, and behavior

(**A**) Schematic representation of the trial events in the odor-sequence task. The initiation of each trial was indicated by the illumination of two overhead houselights. After poking into the central odor port and sampling the presented odor, rats had the option to respond with a 'go' to receive a sucrose reward or a 'no-go' to avoid a prolonged inter-trial interval. (**B**) The six odors were grouped into two sequences, S1 and S2, each consisting of four odor positions (P1–P4). The sequences alternated in a "figure eight" pattern. The numbers at each position represent odor identities, and the blue/red symbols (+/-) indicate rewarded and non-rewarded trials. (**C**) Timeline of the experimental procedure. (**D**) The number of active (solid lines) and inactive (dashed lines) lever presses during sucrose self-administration sessions (upper; n = 3) and cocaine self-administration sessions (lower; n = 3). (**E**) Reconstruction of recording sites, with red squares indicating the locations of electrodes. (**F**) Percentage of correct responses (% correct) are shown for each trial type during single-unit recording sessions. A significant group difference emerged specifically at position P3 between the Sucrose and Cocaine groups ($F_{(1,288)} = 13.1$, $p = 3.4 \times 10^{-4}$, $\eta_p^2 = 0.043$; One-way ANOVA). Blue denotes rewarded trial types, while red denotes non-rewarded trial types. (**G**) Reaction time was defined as the interval between odor port exit and water well entry. For correct no-go trials, where no movement toward the water well was made, a fixed reaction time of 2 seconds—the full response window—was assigned. Reaction time differed significantly between the Sucrose and Cocaine groups overall ($F_{(1,1158)} = 6.6$, $p = 0.01$, $\eta_p^2 = 0.006$; One-way ANOVA), with position-specific analyses revealing significant differences at P1, P3, and P4 (P1: $F_{(1,288)} = 152.9$, $p = 1.9 \times 10^{-28}$, $\eta_p^2 = 0.35$; P3: $F_{(1,288)} = 9.3$, $p = 2.5 \times 10^{-3}$, $\eta_p^2 = 0.03$; P4: $F_{(1,288)} = 139.6$, $p = 1.6 \times 10^{-26}$, $\eta_p^2 = 0.33$; One-way ANOVA). (**H**) Poke latency, measured as the time from light onset to odor port entry. Significant group differences were found across positions ($F_{(1,1158)} = 4.0$, $p = 0.04$, $\eta_p^2 = 0.004$; One-way ANOVA), with specific differences emerging at positions P2, P3, and P4 (P2: $F_{(1,288)} = 10.0$, $p = 1.7 \times 10^{-3}$, $\eta_p^2 = 0.034$; P3: $F_{(1,288)} = 12.4$, $p = 5.0 \times 10^{-4}$, $\eta_p^2 = 0.04$; P4: $F_{(1,288)} = 5.7$, $p = 0.018$, $\eta_p^2 = 0.02$; One-way ANOVA). (**I**) For the absolute S2–S1 difference in reaction time across positions between Sucrose and Cocaine groups, two-way ANOVA revealed significant main effects of group ($F_{(1,572)} = 6.4$, $p = 0.012$, $\eta_p^2 = 0.01$) and position ($F_{(3,572)} = 3.3$, $p = 0.021$, $\eta_p^2 = 0.017$). Black circles denote sucrose data, with shading that deepens progressively from P1 through P4. Cocaine data are indicated by red circles, with coloration shifting from light to dark red across positions P1 to P4. (**J**) Two-way ANOVA revealed significant main effects of group ($F_{(1,572)} = 5.6$, $p = 0.018$, $\eta_p^2 = 0.01$) and position ($F_{(3,572)} = 37.7$, $p = 3.2 \times 10^{-22}$, $\eta_p^2 = 0.16$) on the absolute poke latency difference between S1 and S2 in Sucrose and Cocaine groups. Sucrose data are plotted as graded black circles, with shading progressing from light to dark across positions P1 to P4. Cocaine data are plotted as graded red circles, with shading progressing from light red to dark red across positions P1 to P4. Error bars represent standard errors of the mean (SEMs). *$p < 0.05$; **$p < 0.01$; ***$p < 0.001$.

Figure 2. Discriminating sequences S1 versus S2 at single-unit level

(A-D) Heatmaps showing the activity of individual OFC neurons. Each panel illustrates the firing pattern of a single neuron, capturing its response dynamics across task epochs. Each small grid represents one epoch at a specific position, arranged in the direction of the arrow following the sequence: ["ITI-a", "Light", "Poke", "Odor", "Unpoke", "Choice", "Outcome", "Post-Out", "ITI-b"], repeated for all four positions of each sequence. The left columns represent single OFC neurons from the Sucrose group, where the intensity of left-side epochs closely matches that of the right-side epochs, indicating strong generalization. In contrast, the Cocaine group shows comparatively weaker generalization across sides. S1, sequence 1; S2, sequence 2. (**E**) Percentage of neurons selective at each position in S1 versus S2 in the Sucrose (upper panel) and Cocaine (lower panel) groups. The selectivity was calculated for different task epochs ["ITI-a", "Light", "Poke", "Odor", "Unpoke", "Choice", "Outcome", "Post-Out", "ITI-b"] for all four positions (one-way ANOVA). Epochs within the red dashed boxes indicate selectivity exceeds a 95% confidence interval (CI) (Sucrose: χ^2's > 5.4; p's < 0.02; Cocaine: χ^2's > 4.0; p's < 0.05; Chi-squared test). The p-values were not corrected, and the dotted lines represent the chance level of selectivity according to this criterion. Notably, rats could discriminate between the two sequences (S1 vs. S2) based solely on current sensory information at two task epochs ["Odor" at P3 and P4; black bars]. At all other task epochs, indicated by gray bars, the discrimination relied on an internal memory of events. (**F**) Line plot showing neuronal selectivity at each position in S1 versus S2 for each neuron in both the Sucrose (black line) and Cocaine (red line) groups. The selectivity was calculated at different task epochs for all four positions. Each asterisk indicates that there are significant differences between the two groups (χ^2's > 4.8; p's < 0.03; Chi-squared test). *p < 0.05; error bars are standard deviations (SDs).

Figure 3. Cocaine use reduces the ability of OFC to generalize task-irrelevant odor-overlapping sequences.

(**A**) Decoding accuracy of S1 versus S2 was evaluated within each of the nine task epochs for positions P1 to P4. Error bars represent SDs, and each asterisk indicates that the mean decoding accuracy exceeds a 95% confidence interval calculated using the same decoding process with label-shuffled data. The dotted lines represent the chance level of decoding. The meaning of the black bars is consistent with **Figure 2E**. (**B**) Decoding accuracy of S1 versus S2 at each position was assessed using varying ensemble sizes for the Sucrose (black) and Cocaine (red) groups across all epochs. The Cocaine group demonstrated higher decoding accuracy and reduced generalization of task-irrelevant, overlapping sequences compared to the Sucrose group ($F_{(1,118)} = 16.8$, $p = 7.8 \times 10^{-5}$, $\eta_p^2 = 0.12$; One-way ANOVA). P1, P2, P3, and P4 represent positions 1, 2, 3, and 4, respectively. (**C**) Decoding accuracy of S1 versus S2 at each position was assessed using varying ensemble sizes for the Sucrose group (black, same data as in **Figure 3B**) and the Less Training group (blue, Zhou et al., 2021) across all epochs. The decoding accuracy in the Less Training group was comparable to that observed in the Cocaine group (**Figure 3B**, red) ($F_{(1,118)} = 0.01$, $p = 0.92$, $\eta_p^2 = 9.0 \times 10^{-5}$; One-way ANOVA). Additionally, the Less Training group exhibited significantly higher decoding accuracy than the Sucrose group ($F_{(1,118)} = 18.1$, $p = 4.2 \times 10^{-5}$, $\eta_p^2 = 0.13$; One-way ANOVA). P1, P2, P3, and P4 represent positions 1, 2, 3, and 4, respectively. *p < 0.05; error bars indicate SDs. (**D**) Confusion matrices showing within-sequence position decoding from OFC ensemble activity at four task positions for the Sucrose and Cocaine groups. The y-axis denotes the rats' actual position, and the x-axis indicates the predicted position. Brighter colors reflect higher decoding probabilities. (**E**) Quantification of within-sequence decoding accuracy across positions revealed a significant

difference between groups ($p = 0.027$; $W = 1118$; two-sided Wilcoxon rank-sum test), with Sucrose shown in black and Cocaine in red. (**F**) Confusion matrices showing across-sequence position decoding from OFC ensemble activity at the same four task positions. Axes are as in (**D**), with brighter colors indicating higher decoding probabilities. (**G**) Quantification of across-sequence decoding accuracy also revealed a significant group difference ($p = 0.046$; $W = 1144$; two-sided Wilcoxon rank-sum test), with Sucrose shown in black and Cocaine in red.

Figure 4. Cocaine use impairs the OFC's function in temporal cognition and decreases the generalization of task-irrelevant odor-overlapping sequences

(**A-B**) Ten components of TCA applied to Sucrose(**A**) and Cocaine(**B**) neuron activity are displayed. Each component consists of a neuron factor (left column), a temporal factor spanning nine events with eight time points per event (middle column), and a trial factor (right column). Temporal factors are grouped as follows: 1–8 (preTrial), 9–16 (Light), 17–24 (Poke), 25–32 (Odor), 33–40 (Unpoke), 41–48 (Choice), 49–56 (Outcome), 57–64 (postTrial1), and 65–72 (postTrial2). The dataset includes eight trial types, each with 40 trials. Trial factors 1–80 and 241–320 represent rewarded (positive) trials, while 81–240 correspond to unrewarded (negative) trials. Trials are further categorized as follows: 1–80 (P1), 81–160 (P2), 161–240 (P3), and 241–320 (P4). These low-dimensional components were extracted from a 10-component model for both the Sucrose(**A**) and Cocaine groups(**B**). In the Sucrose group, components 1, 6, 7, and 10 encode positive trials, while components 2, 3, and 8 encode negative trials. Similarly, in the Cocaine group, components 1, 4, 6, 7, and 10 encode positive trials, whereas components 2, 3, 5, 8, and 9 encode negative trials. Notably, in the Sucrose group, beyond reward-related components, additional components encode aspects of temporal cognition (components 5 and 9), along with early components broadly active across most trials (component 4). (**C**) Plot illustrating mutual information (MI) between across-trial factors and trial types. The Sucrose group exhibits lower MI, particularly at components 5 and 9. A two-way ANOVA confirmed a significant reduction in MI for the Sucrose group ($F_{(1,1360)} = 571.6$, $p = 9.7 \times 10^{-106}$, $\eta_p^2 = 0.3$), especially at these components, which showed consistent patterns across all trial types, aligning with the plots in (**A**) of the Sucrose group, indicating a weaker dependency between across-trial factors and trial types. A significant difference was also observed across components ($F_{(9,1360)} = 266.3$, $p = 1.2 \times 10^{-292}$, $\eta_p^2 = 0.64$). (**D**) Plot illustrating mutual information (MI) between across-trial factors and time. The Sucrose group demonstrates greater MI, particularly at components 5 and 9, suggesting a stronger dependency between across-trial factors and time. A two-way ANOVA confirmed a significant increase in MI for the Sucrose group ($F_{(1,1360)} = 850.1$, $p = 1.4 \times 10^{-145}$, $\eta_p^2 = 0.38$). Additionally, a significant difference was observed across components ($F_{(9,1360)} = 176.8$, $p = 1.4 \times 10^{-221}$, $\eta_p^2 = 0.54$). Error bars are SEM.

Figure 3—figure supplement 1. The ability of the OFC to generalize task-irrelevant odor-overlapping sequences decreases as learning progresses

(**A**) Organization of sixteen odors into two pairs of sequences (S1a-S1b and S2a-S2b), with each sequence consisting of six trials or positions (P1-P6). The blue '+' symbol represents rewarded trials, while the red '-' symbol represents non-rewarded trials. Odor identities are represented by numbers 0-15, and arrows indicate transitions between sequences. (**B-C**) The percentage of

decoding accuracy was analyzed across different groups with varying training days and ensemble sizes. Significant differences were observed between S1a and S1b across all time periods (days 1–5, days 6–10, and days 11–15) for different numbers of selected neurons ($F_{(2,42)} = 11.2$, $p = 1.3 \times 10^{-4}$, $\eta_p^2 = 0.35$). In contrast, no significant differences were found between S2a and S2b ($F_{(2,42)} = 0.17$, $p = 0.84$, $\eta_p^2 = 8.2 \times 10^{-3}$). Additionally, significant differences were identified between S1 and S2 ($F_{(1,88)} = 8.69$, $p = 4.1 \times 10^{-3}$, $\eta_p^2 = 0.09$). The error bars indicate SDs.

24-Position Odor Sequence Task

Rats were trained in 18" x 18" aluminum behavioral chambers equipped with an odor port and a fluid well for odor and sucrose delivery, respectively. Odor and fluid delivery were controlled by solenoids via a custom C++ program. Infrared beam sensors monitored entries into both ports. Each trial was cued by the illumination of two house lights in the front wall above the odor panel. Rats initiated a trial by nose-poking into the odor port within 5 seconds of light onset. Upon successful initiation, an odor was delivered after a 500-ms delay and continued until the rat withdrew. Trials were aborted if the rat exited the port before 500 ms. Otherwise, after withdrawal, the rat had 2 seconds to respond at the fluid well.

On rewarded trials, a correct response at the well triggered sucrose delivery (10% w/v; 50 μL) after a variable delay (400–1500 ms). The trial ended when the rat left the well, at which point the house lights turned off, initiating the inter-trial interval (ITI). If no response was made within the 2-s window, or if the rat responded on a non-rewarded trial (a rare occurrence), the trial also ended without reward. Correct responses were followed by a 4-s ITI; incorrect responses led to an 8-s ITI.

Odors were drawn from a pool of 16 and organized into four sequences: S1a, S1b, S2a, and S2b. Rewarded (+) and non-rewarded (–) trials were defined by the following sequence structures:

S1a: 0+, 1–, 4–, 5+, 6–, 7+

S1b: 2+, 3–, 4–, 5+, 6–, 7+

S2a: 8+, 9–, 12–, 13+, 14–, 15+

S2b: 10+, 11–, 12–, 13–, 14+, 15+

Training proceeded in stages. Rats were first shaped to poke into the odor port and then respond at the fluid well. They were initially trained on a single odor pair (one rewarded, one not) from sequence S1a or S1b. Sessions contained up to 480 trials. Once rats achieved >90% correct performance, additional odor pairs were gradually introduced until they performed reliably on full S1a and S1b sequences. Next, rats were trained to discriminate odors 13 and 14 from sequence S2, including multiple reversals of their reward valence. Once they achieved >75% accuracy across trial types and completed three reversals, the remaining odors from S2a and S2b were added. In the final training phase, rats performed sessions with all four sequences (S1a, S1b, S2a, S2b). Each sequence was presented 20 times per session (480 trials total), with transitions between S1 and S2 sequences occurring in a pseudo-random order. S1 sequences were followed by S2 with ~55%/45% probability (2a/2b), and S2 sequences were followed by S1 with ~67%/37% probability (1a/1b). This sequence structure was repeated throughout each session.

Prior to electrode implantation, rats were trained on the full task for at least three weeks and had to reach >75% accuracy on all trial types.

Figure 3—figure supplement 2. Two-way ANOVA of sequence and position effects

(**A–B**) Percentage of neurons showing significant effects of sequence or interaction in the Sucrose (**A**) and Cocaine (**B**) groups. No significant sequence or interaction effects were detected across any epoch in the Sucrose group ($\chi^2 < 6.5$, $p > 0.06$; Chi-squared test). In contrast, the Cocaine group showed a markedly higher proportion of neurons exhibiting interaction effects than sequence effects during the Light, Poke, Odor, Post-Out, and ITIb epochs ($\chi^2 > 5.5$, $p < 0.034$; Chi-squared test). (**C**) Percentage of neurons showing sequence effects. A significant group difference was observed only at the ITIb epoch ($\chi^2 = 11$, $p = 8.3 \times 10^{-3}$; Chi-squared test). (**D**) Percentage of neurons showing position effects. Significant group differences were found at the epochs of Poke, Odor, Unpoke, Choice, Outcome, and ITIb ($\chi^2 > 13.8$, $p < 3.0 \times 10^{-4}$; Chi-squared test). (**E**) Percentage of neurons showing interaction effects. The Cocaine group showed significantly more interaction effects than the Sucrose group at epochs of Poke, Odor, Post-Out, and ITIb ($\chi^2 > 14.5$, $p < 4.2 \times 10^{-4}$; Chi-squared test).

Figure 3—figure supplement 3. Correlation of preferred positions

Plots display regression lines for the Sucrose and Cocaine groups. The black line represents the Sucrose group, while the dark red line corresponds to the Cocaine group. A statistical comparison using Fisher's r-to-z transformation revealed a significant difference between the two groups ($z = 4.92$, $p = 8.6 \times 10^{-7}$). P1, P2, P3, and P4 denote different positions.

Figure 4—figure supplement 1. Error and similarity plots for TCA

The optimization landscape of TCA may contain suboptimal solutions (local minima), necessitating iterative optimization to minimize a cost function. To evaluate the stability of this process, we generated error and similarity plots. Specifically, we ran the TCA optimization algorithm 100 times for 10 components, each initialized with random conditions, and plotted the normalized reconstruction error across all runs. This approach enabled us to assess whether certain runs converged to local minima with high reconstruction errors. As shown in **Figure 4—figure supplement 1A-B** (left panels), the error plots indicate that all 100 runs at a fixed number of components produced nearly identical reconstruction errors. Additionally, models with 9 and 10 components exhibited very similar errors. The similarity plot (**Figure 4—figure supplement 1A-B**, right panel) further quantifies the consistency of TCA models across different component numbers (horizontal axis). For each model, similarity scores were computed relative to the best-fit model with the same number of components, with the lines representing the mean similarity as a function of the number of components. Across all tested component numbers, the 100 repeated runs per component showed substantial overlap and consistently yielded similarity scores above 0.8, indicating high quantitative consistency. Our tests indicate that adding more than ten components reduces model reliability, making them less identifiable. (**A-B**) Error plots (left panel) and similarity

plots (right panel) for Sucrose (**A**) and Cocaine group(**B**). Error plots illustrate the normalized reconstruction error across TCA models with varying component numbers. Each black dot corresponds to a model fit using different initial parameters, all of which produced nearly identical performance. Notably, reconstruction error showed almost no further improvement beyond ten components for both groups. The similarity plot displays the similarity score for TCA models with different component numbers. Each black dot represents the similarity of a given model to the best-fit model with the same number of components, demonstrating high repeatability for both groups.

Figure 4—figure supplement 2. Four component model, cocaine impairs OFC temporal cognition and sequence generalization with irrelevant overlapping odors

(**A**–**B**) Four components from TCA applied to Sucrose (**A**) and Cocaine (**B**) neuron activity are shown. Each component includes a neuron factor (left), a temporal factor spanning 72 time points across nine events (middle), and a trial factor (right). Temporal events are grouped as: 1–8 (preTrial), 9–16 (Light), 17–24 (Poke), 25–32 (Odor), 33–40 (Unpoke), 41–48 (Choice), 49–56 (Outcome), 57–64 (postTrial1), and 65–72 (postTrial2). The dataset contains eight trial types (40 trials each): trials 1–80 and 241–320 are rewarded (P1, P4), and 81–240 are unrewarded (P2, P3). In Sucrose, components 1, and 2. In Cocaine, components 1, 2, and 4 encode positive trials; 3 encode negative trials. Additionally, Sucrose components 3 and 4 relate to temporal cognition. (**C**) Mutual information (MI) between across-trial factors and trial types is lower in the Sucrose group, especially at components 1, 3 and 4, indicating weaker dependency. Two-way ANOVA confirmed a significant group difference ($F_{(1,544)} = 1074.5$, $p = 6.7 \times 10^{-131}$, $\eta_p^2 = 0.66$) and component effect ($F_{(3,544)} = 17.7$, $p = 5.2 \times 10^{-11}$, $\eta_p^2 = 0.089$). (**D**) MI between across-trial factors and time is higher in Sucrose, particularly at components 1, 2 and 4, reflecting stronger temporal encoding. ANOVA showed a significant group effect ($F_{(1,792)} = 36.5$, $p = 2.3 \times 10^{-9}$, $\eta_p^2 = 0.044$) and component effect ($F_{(3,792)} = 6.5$, $p = 2.4 \times 10^{-4}$, $\eta_p^2 = 0.024$). Error bars denote SEM.

Figure 4—figure supplement 3. Fourteen component model, cocaine use impairs OFC function in temporal cognition and hinders generalization across odor-overlapping, task-irrelevant sequences

(**A**–**B**) Fourteen components from TCA applied to Sucrose (**A**) and Cocaine (**B**) neural activity are shown. Each component includes a neuron factor (left), a temporal factor spanning nine events with eight time points each (middle), and a trial factor (right). Temporal segments are grouped as: preTrial (1–8), Light (9–16), Poke (17–24), Odor (25–32), Unpoke (33–40), Choice (41–48), Outcome (49–56), postTrial1 (57–64), and postTrial2 (65–72). The dataset comprises eight trial types (40 trials each): rewarded trials (1–80, 241–320; P1, P4) and unrewarded trials (81–240; P2, P3). Low-dimensional components were extracted from a 14-component model for each group. In Sucrose, components 2, 7, 8, 12 and 13 encode positive trials; components 1, 4, 10, 11 and 14 encode negative trials. In Cocaine, positive trial components are 2, 3, 5,7, 8, 11, 12, and 13; negative trials are encoded by components 1, 4, 6, 9, 10, and 14. Additionally, Sucrose components 3, 5 and 6 encode temporal structure, and component 9 is broadly active across trials. (**C**) Mutual information (MI) between across-trial factors and trial types is lower in the Sucrose group, particularly at components 3, 5 and 6, indicating weaker encoding of trial identity. A two-way ANOVA confirmed a significant group difference ($F_{(1,308)} = 571.6$, $p = 4.1 \times 10^{-25}$, $\eta_p^2 = 0.29$) and component effect (F

$_{(13,308)}$ 33.0, $p = 1.0 \times 10^{-50}$, $\eta_p^2 = 0.58$). (**D**) MI between across-trial factors and time is higher in Sucrose, especially at components 5 and 9, reflecting stronger temporal encoding. A two-way ANOVA revealed a significant group effect ($F_{(1,2772)} = 3.8$, $p = 0.046$, $\eta_p^2 = 0.0014$) and component effect ($F_{(13,2772)} = 5.5$, $p = 5.6 \times 10^{-10}$, $\eta_p^2 = 0.025$). Error bars represent SEM.

Figure 4—figure supplement 4. Ten-component model for individual Sucrose rats

(**A**, **C**, **E**) Ten-component TCA models are presented for neuronal activity recorded from individual sucrose-trained rats. Each component comprises three factors: a neuron factor (left column), a temporal factor spanning nine task events with eight time points per event (middle column), and a trial factor (right column). Temporal factors are organized as follows: 1–8 (preTrial), 9–16 (Light), 17–24 (Poke), 25–32 (Odor), 33–40 (Unpoke), 41–48 (Choice), 49–56 (Outcome), 57–64 (postTrial1), and 65–72 (postTrial2). The dataset includes eight trial types with 40 trials each. Trial factors 1–80 and 241–320 correspond to rewarded (positive) trials, while 81–240 correspond to unrewarded (negative) trials. Trials are further categorized by position: 1–80 (P1), 81–160 (P2), 161–240 (P3), and 241–320 (P4). These low-dimensional components reflect the latent structure of population activity. Across Sucrose rats #J505, #J506, and #J507, several TCA components consistently distinguished trial valence. Components 3, 4, and 9 were associated with positive trials in all three rats, with components 6 and 7 additionally contributing in #J505 and #J506. Negative trials were reliably encoded by components 5 and 8 across all rats, with component 6 also contributing in #J507. Furthermore, each rat exhibited temporal components (typically 2 and 10, with 7 also involved in #J507) and a broadly active early component (1) that was consistent across trial types. (**B**, **D**, **F**) Error plots (left panels) and similarity plots (right panels) are shown for each Sucrose rat. The error plots demonstrate that all 100 runs with a fixed number of components yielded nearly identical reconstruction errors, indicating stable model convergence. Models with 9 and 10 components produced similarly low errors, with minimal improvement beyond 10 components. The similarity plots quantify consistency across model runs. For each component number, similarity was computed relative to the best-fit model, and mean similarity is plotted as a function of component number. Across all tested component counts, repeated runs produced high similarity scores (generally > 0.8), indicating that the decomposition was highly stable and reproducible for all Sucrose rats.

Figure 4—figure supplement 5. Ten-component TCA model applied to individual rats from the Cocaine group

(**A**, **C**, **E**) TCA-derived ten-component models are shown for individual Cocaine rats. Each component includes a neuron factor (left), a temporal factor spanning nine task events (middle), and a trial factor (right). Temporal factors cover preTrial (1–8), Light (9–16), Poke (17–24), Odor (25–32), Unpoke (33–40), Choice (41–48), Outcome (49–56), postTrial1 (57–64), and postTrial2 (65–72). The dataset includes eight trial types (40 trials each): trials 1–80 and 241–320 are rewarded (positive), and 81–240 are unrewarded (negative), grouped by position (P1–P4). In the Cocaine rats, positive trials were consistently encoded by components 1, 3, 4, 6, 9, and 10. Negative

553 trials were represented by components 2, 5, and 8 across all Cocaine rats, with component 7
554 additionally contributing to rats #J509 and #510. (**B**, **D**, **F**) Error plots (left) and similarity plots
555 (right) are shown for each Cocaine rat. The error plots indicate that across 100 runs with a fixed
556 number of components, reconstruction errors were nearly identical, demonstrating stable model
557 convergence. Models with 9 or 10 components achieved comparably low errors, with little
558 improvement beyond 10 components. The similarity plots quantify consistency across runs: for
559 each component count, similarity was calculated relative to the best-fit model, and mean similarity
560 is plotted as a function of component number. Across all component counts, repeated runs yielded
561 high similarity scores (generally >0.8), confirming that the decomposition was stable and
562 reproducible in all sucrose rats.

563

ACKNOWLEDGMENTS

This research was funded by the Intramural Research Program at the National Institute on Drug Abuse (ZIA-DA000587). The views expressed in this article are solely those of the authors and do not necessarily represent the opinions of the NIH or DHHS.

AUTHOR CONTRIBUTIONS

J.Z. and G.S. designed the experiments, while J.Z. and W.Z. collected and analyzed the data with guidance and technical support from Z.Z and L.E.M.. W.Z., J.Z., and G.S. wrote the manuscript, incorporating feedback from all authors.

DECLARATION OF INTERESTS

The authors declare no competing interests.

STAR METHODS

KEY RESOURCES TABLE

In a separate file.

CONTACT FOR REAGENT AND RESOURCE SHARING

This study did not generate any unique reagents. However, for further information or requests for resources and reagents, please contact the Lead Contact, Geoffrey Schoenbaum (geoffrey.schoenbaum@nih.gov).

EXPERIMENTAL MODEL AND SUBJECT DETAILS

The study was conducted on a group of six male Long-Evans rats (Charles River strain), aged around three months and weighing between 175–200 g. The rats were housed individually in an AAALAC-accredited animal care facility at the National Institute on Drug Abuse Intramural Research Program (NIDA-IRP), with *ad libitum* access to food on a 12-hour light-dark cycle. Water was removed a day before testing, and the rats were provided with free access to water for 10 minutes each afternoon in their home cages. If there was no testing scheduled for the following day, they were given free access to water. All behavioral testing was conducted at the NIDA-IRP, and the animal care and experimental procedures were conducted in accordance with the guidelines set by the US National Institutes of Health (NIH) and approved by the Animal Care and Use Committee (ACUC) at the NIDA-IRP.

METHOD DETAILS

Behavioral Tasks

Figure 8 Task

The study employed aluminum boxes (18 in. on a side) equipped with a port for odor delivery and a well for delivery of sucrose solution for conducting behavioral training. A custom-written C++ program and a system of relays and solenoid valves were used to control the task events. The entries into the odor port and the fluid well were detected by infrared beam sensors. The availability of each trial was signaled by the illumination of two house lights above the odor port. The trial was initiated if the rat entered the odor port within 5 s after light onset, leading to odor delivery after a 500-ms delay. The rats were required to remain in the port for an additional 500 ms; otherwise, the trial was aborted, and the lights extinguished. After 500 ms, the rats were free to leave the port, terminating odor delivery. Post port exit, the rats had 2 s to respond at the fluid well. Responding on rewarded trials led to the delivery of a sucrose solution (10% w/v; 50 μL) after a random delay ranging from 400 to 1,500 ms. On nonrewarded trials, nonresponding during the 2-s

period, or responding after the 2 s, the house lights were extinguished, indicating the end of the trial and the beginning of the ITI. Correct trials were followed by a 4-s ITI, and trials on which the rat made an error were followed by an 8-s ITI.

The study for the Figure 8 task included six odors, organized into two sequences (S1 and S2) that occurred repeatedly in turn (S1→S2→S1→S2→⋯→S1→S2; 40 repeats of each sequence). On each trial, one of six odors was delivered to the odor port. The odor identity is indicated by a number, and reward and nonrewarded are indicated by the positive (+) and negative (−) symbols, orders of the odors were organized and showed below:

S1: 5+, 0−, 1−, 2+

S2: 3+, 0−, 1−, 4+

To avoid bias, the starting sequence for each session—either S1 or S2—was determined in a fully pseudorandom manner. Before training with any odors, rats were first shaped to nosepoke at the odor port and then respond at the well for a reward. The rats were trained on the full set of sequences from Day 1 until they achieved >75% accuracy on every trial type in a session. Following this, electrode arrays were implanted bilaterally in the orbitofrontal cortex.

To clarify, the animals were not initially trained on the "Figure 8" task (which involves six odors across two four-odor sequences, S1 and S2) prior to exposure to the full 24-position task. Each rat in this study was trained and recorded on only one behavioral paradigm—either the Figure 8 task or the 24-Position Odor Sequence Task, but not both. These tasks were conducted in separate cohorts of animals. All data presented in the figures of this manuscript were obtained from the Figure 8 task, using sucrose-trained, cocaine-trained, or previously reported minimally trained animals, with the exception of Figure 3—figure supplement 1. The data shown in Figure 3—figure supplement 1, derived from the 24-Position Odor Sequence Task, were published previously, and the behavioral paradigm is described in the corresponding figure legend.

Surgical Procedures

Rats were surgically implanted with a total of 32 electrodes, organized into two bundles of 16 electrodes each. These bundles were constructed using nickel-chromium wires with a bare diameter of 25 µm (AM Systems, WA). The implantation targeted the bilateral orbitofrontal cortices (AP: 3 mm, ML: 3.2 mm). To ensure proper placement, each wire bundle was encased in a 27-gauge stainless-steel tubing and trimmed using fine spring scissors. The trimmed wires extended approximately 1.5-2 mm beyond the tubing's end. Initially, the wire tips were positioned 4.2 mm ventral from the brain surface. Following the surgical procedure, the rats received oral doses of Cephalexin (15 mg/kg) twice daily for a duration of two weeks to prevent any potential infections.

Catheter Surgery

Rats used for cocaine self-administration received chronic indwelling jugular catheter implants (Instech Laboratories). Rats were anaesthetized using ketamine (100 mg/kg, i.p., Sigma) and xylazine (10 mg/kg, i.p., Sigma). Blunt dissection was performed to isolate right external jugular veins and catheters were surgically implanted 3 cm into the veins. Catheters were passed subcutaneously to the back, where they were attached to an external harness. Carprofen (5 mg/kg,

653 s.c., Pfizer) was administered after surgery as an analgesic. Rats recovered for 7 days before self-
654 administration began. During recovery and self-administration, catheters were flushed daily with a
655 cocktail of enrofloxacin (4.0 mg/mL, Bayer) and heparinized saline (50 IU/mL in 0.9% sterile saline,
656 Sigma) to maintain catheter patency.

657 **Self-Administration**

658 Following recovery from catheterization surgery, rats were trained to self-administer cocaine-HCl
659 (0.75 mg/kg/infusion; n = 3) or sucrose (10% wt/vol; n = 3) for 14 consecutive days. Rats were
660 trained in modular behavioral test chambers (Coulbourn Instruments) housed in sound-attenuating
661 boxes. Each chamber was equipped with two levers positioned 8 cm above the floor on opposite
662 sides of the same wall. For intravenous cocaine self-administration, catheter ports were attached to
663 silastic tubing connected to infusion pumps (Med Associates Inc.) located outside sound-
664 attenuating boxes. For sucrose self-administration, sucrose solution was delivered via photobeam-
665 monitored recessed dippers. Daily sessions were 3 hours and began with the illumination of a
666 house light and the insertion of an active lever. Under a fixed ratio 1 (FR1) schedule of
667 reinforcement, active lever presses resulted in 4 s infusions or dipper insertions (0.05 mL), for
668 cocaine-HCl or sucrose, respectively, and were paired with the illumination of a cue light above the
669 active lever. Infusions and dipper insertions were followed by a 40 s timeout period when the
670 active lever retracted and the house light was extinguished. Following the timeout period, the lever
671 was reinserted and the house light was turned back on. Inactive lever presses had no programmed
672 consequence. Reinforcers were limited to 20 *per* hour to prevent overdose in cocaine self-
673 administering rats. When 20 reinforcers were earned in less than an hour, a timeout period as
674 described above was imposed until the beginning of the next hour.

675 **Single-Unit Recording**

676 Electrophysiological signals were recorded using Plexon OmniPlex systems (Plexon, Dallas, TX).
677 These signals were digitized, amplified, and subjected to bandpass filtering (250–8,000 Hz) to
678 isolate spike activity. Manual thresholding was performed on each active channel to capture
679 unsorted spikes. Timestamps for behavioral events were synchronized with the Plexon system and
680 recorded together with the neural activity. To remove noise and identify single units, spike sorting
681 was carried out offline using Offline Sorter (v.4.0; Plexon), utilizing a template-matching algorithm.
682 The sorted files were then processed in NeuroExplorer (Nex Technologies, Colorado Springs, CO) to
683 extract timestamps for both unit activity and behavioral events. Subsequently, these timestamps
684 were exported as MATLAB (2021b; MathWorks) formatted files for further analysis. It is important
685 to note that the electrodes were not advanced within a specific problem. However, we cannot make
686 any claims regarding the consistency of single units recorded on different days within the same
687 problem, as they may represent distinct neurons. To sample different neural populations during
688 odor problems, the electrodes were advanced by approximately 120 µm. Both in vivo recordings
689 and spike sorting were performed in a blinded manner, without knowledge of whether the subject
690 belonged to the Sucrose or Cocaine group.

691

692 **QUANTIFICATION AND STATISTICAL ANALYSES**

693 Quantification and statistical analyses were conducted using MATLAB (R2024b; MathWorks) and
694 Python Software Foundation, 2024. The sample sizes of rats and neurons were not predetermined

through specific statistical methods; however, they are consistent with those reported in previous studies conducted by our lab and other research groups.

Task Events and Peri-Event Spike Train Analysis

The trials were divided into nine distinct epochs, each corresponding to different task events: "ITI-a", "Light", "Poke", "Odor", "Unpoke", "Choice", "Outcome", "postOutcome", and "ITI-b". "ITI-a" represented the time point 0.7 seconds before the house-light turned on. On reward trials, the well-entry moment was labeled "Choice." The "Outcome" epoch denoted the time of reward delivery. On non-reward trials, the end of the 2-second response window was marked as "Choice," and a time point 0.7 seconds after "Choice" was labeled as "Outcome." Both on reward and non-reward trials, 0.7 seconds after the outcome was recorded as "postOutcome," followed by another 0.7 seconds designated as "ITI-b." Behavioral performance was evaluated by calculating the percentage of trials in which the rats responded correctly and determining the latency at which they initiated a trial after the onset of the light. The spike train for each isolated single unit was aligned to the onset of each task event to create a peri-event time histogram (PETH). The PETH was constructed with a pre-event time of 200 ms and a post-event time of 600 ms, counting the number of spikes within each 100 ms bin. To smooth the PETH on each trial, a Gaussian kernel with a σ (standard deviation) of 50 ms was applied. For further analysis, a random selection of 30 correct trials was made from each trial type, resulting in a total of 240 trials (30 trials × 8 trial types). The post-event firing rates (100–600 ms) were averaged to obtain a single measure of neural activity for each neuron on each trial during each task epoch.

Classification Analyses

The neural data collected during each task epoch were organized into a two-dimensional matrix, where the rows represented individual trials and the columns represented the firing rates of each neuron across all trials. In other words, each trial was represented as a vector, with each dimension corresponding to the firing rate of a specific neuron. Neurons recorded across different sessions were concatenated, aligning them with the corresponding trials to create pseudoensembles. To remove temporal correlations between neurons and generate different pseudoensembles, we shuffled the trial orders within each trial type. This shuffling process was repeated 10,000 times, resulting in 10,000 pseudoensembles. By using the linear Support Vector Machine (SVM) for classification analyses, we assessed the classification accuracy through a leave-one-out cross-validation procedure. Specifically, one trial from each trial type was excluded for future testing, while the remaining trials were used to train the classifier. For each pseudoensemble, the leave-one-out cross-validation was repeated 200 times to estimate the mean decoding accuracy. The decoding analyses were conducted on the 10,000 pseudoensembles to calculate an overall mean decoding accuracy. To determine the statistical significance of the overall mean decoding accuracy, we estimated a 95% confidence interval by running the same decoding process with label-shuffled pseudoensembles.

Cross-sequence decoding

To assess population decoding of position within and across sequences in OFC cells (n = 1000), we applied a Support Vector Machine (SVM) classifier. Decoding accuracy was estimated using a leave-one-out cross-validation approach. In each iteration, 30 trials per trial type were randomly sampled

for each of the 9 task epochs, producing a 120 (trials) × 9 (epochs) matrix per sequence. One trial from each trial type in sequence 1 was withheld for testing, while the trial with the corresponding index in sequence 2 was simultaneously set aside for across-sequence evaluation. The classifier was trained on the remaining sequence 1 trials. For each epoch and trial type, decoding accuracy was averaged across 1000 iterations to obtain the mean performance.

TCA Analysis

To perform TCA, neuronal firing rates for each group were structured into a three-dimensional array ($N \times T \times K$), where N represents the number of neurons, T the time samples *per* trial, and K the number of experimental trials. This array, referred to as a third-order tensor, captures neuronal activity across trials. Data were exported as a MATLAB .mat file and imported into Spyder for analysis using the TensorTools package [20]. Temporal factors were grouped as follows: factors 1–8 (preTrial), 9–16 (Light), 17–24 (Poke), 25–32 (Odor), 33–40 (Unpoke), 41–48 (Choice), 49–56 (Outcome), 57–64 (postTrial1), and 65–72 (postTrial2). There are 8 trial types, each with 40 trials. Trial factors 1–80 and 241–320 represent positive trials with reward, while 81–240 correspond to negative trials without reward. Trials 1–80 map to P1, 81–160 to P2, 161–240 to P3, and 241–320 to P4. Error and similarity plots were generated to assess the stability of TCA's optimization landscape. Specifically, we ran the TCA optimization algorithm 100 times for each of 10 components, initializing each run with random conditions, and plotted the normalized reconstruction error across all iterations. This approach allowed us to evaluate whether certain runs converged to local minima with high reconstruction errors. Additionally, similarity scores were computed for each model relative to the best-fit model with the same number of components, with the lines representing the mean similarity as a function of component count. Across all tested component numbers, the 100 repeated runs exhibited substantial overlap and consistently produced similarity scores above 0.8, demonstrating high quantitative consistency. MI was calculated for across-trial factors and trial type, as well as across-trial factors and time, after aligning components between the Sucrose and Cocaine groups. The alignment followed the same ordering of across-temporal factors between the two groups. MI was calculated for across-trial factors and trial type, as well as across-trial factors and time, after aligning components between the Sucrose and Cocaine groups. The alignment followed the same ordering of across-temporal factors between the two groups.

Data and code availability

All data and analysis code associated with this study are available on OSF at https://osf.io/azvhm/overview.

References

1. Moneta, N., Grossman, S., and Schuck, N.W. (2024). Representational spaces in orbitofrontal and ventromedial prefrontal cortex: task states, values, and beyond. Trends in Neurosciences *47*, 1055-1069.
2. Bein, O., and Niv, Y. (2025). Schemas, reinforcement learning and the medial prefrontal cortex. Nature Reviews Neuroscience *26*, 141-157.
3. Samborska, V., Butler, J.L., Walton, M.E., Behrens, T.E.J., and Akam, T. (2022). Complementary task representations in hippocampus and prefrontal cortex for generalising the structure of problems. Nature Neuroscience *25*, 1314-1326.
4. Farovik, A., Place, R.J., McKenzie, S., Porter, B., Munro, C.E., and Eichenbaum, H. (2015). Orbitofrontal cortex encodes memories within value-based schemas and represents contexts that guide memory retrieval. Journal of Neuroscience *35*, 8333-8344.
5. Morrissey, M.D., Insel, N., and Takehara-Nishiuchi, K. (2017). Generalizable knowledge outweighs incidental details in prefrontal ensemble code over time. eLIFE *6*, e22177.
6. Lin, H., and Zhou, J. (2024). Hippocampal and orbitofrontal neurons contribute to complementary aspects of associative structure. Nature Communications *15*, 5283.
7. Schuck, N.W., Cai, M.B., Wilson, R.C., and Niv, Y. (2016). Human orbitofrontal cortex represents a cognitive map of state space. Neuron *91*, 1402-1412.
8. Wilson, R.C., Takahashi, Y.K., Schoenbaum, G., and Niv, Y. (2014). Orbitofrontal cortex as a cognitive map of task space. Neuron *81*, 267-279.
9. Gardner, M.P.H., and Schoenbaum, G. (2021). The orbitofrontal cartographer. Behavioral Neuroscience *135*, 267-276.
10. Zhou, J., Zong, W., Jia, C., Gardner, M.P.H., and Schoenbaum, G. (2021). Prospective representations in rat orbitofrontal ensembles. Behavioral Neuroscience *135*, 518-527.
11. Grimm, J.W., Hope, B.T., Wise, R.A., and Shaham, Y. (2001). Incubation of cocaine craving after withdrawal. Nature *412*, 141-142.
12. Zhou, J., Gardner, M.P.H., Stalnaker, T.A., Ramus, S.J., Wikenheiser, A.M., Niv, Y., and Schoenbaum, G. (2019). Rat orbitofrontal activity contains multiplexed but dissociable representations of value and task structure in an odor sequence task. Current Biology *29*, 897-907.
13. Jentsch, J.D., and Taylor, J.R. (1999). Impulsivity resulting from frontostriatal dysfunction in drug abuse: implications for the control of behavior by reward-related stimuli. Psychopharmacology *146*, 373-390.
14. Panayi, M.C., Shetty, S., Porod, M., Bahena, L., Zi, Z.-X., Newman, A.H., and Schoenbaum, G. (2024). The selective D3-receptor antagonist VK4-116 reverses loss of insight caused by self-administration of cocaine in rats. Neuropsychopharmacology *49*, 1590-1599.
15. Ersche, K.D., Roiser, J.P., Robbins, T.W., and Sahakian, B.J. (2008). Chronic cocaine but not chronic amphetamine use is associated with perseverative responding in humans. Psychopharmacology *197*, 421-431.
16. Ersche, K.D., Gillan, C.M., Jones, P.S., Williams, G.B., Ward, L.H.E., Luijten, M., de Wit, S., Sahakian, B.J., Bullmore, E.T., and Robbins, T.W. (2016). Carrots and sticks fail to change behavior in cocaine addiction. Science *352*, 1468-1471.
17. Nelson, A., and Killcross, S. (2006). Amphetamine exposure enhances habit formation. Journal of Neuroscience *26*, 3805-3812.
18. Schoenbaum, G., and Setlow, B. (2005). Cocaine makes actions insensitive to outcomes but not extinction: implications for altered orbitofrontal-amygdalar function. Cerebral Cortex *15*, 1162-1169.

19. Radulescu, A., and Niv, Y. (2019). State representation in mental illness. Current Opinion in Neurobiology *55*, 160-166.
20. Williams, A.H., Kim, T.H., Wang, F., Vyas, S., Ryu, S.I., Shenoy, K.V., Schnitzer, M., Kolda, T.G., and Ganguli, S. (2018). Unsupervised discovery of demixed, low-dimensional neural dynamics across multiple timescales through tensor component analysis. Neuron *98*, 1099-1115.

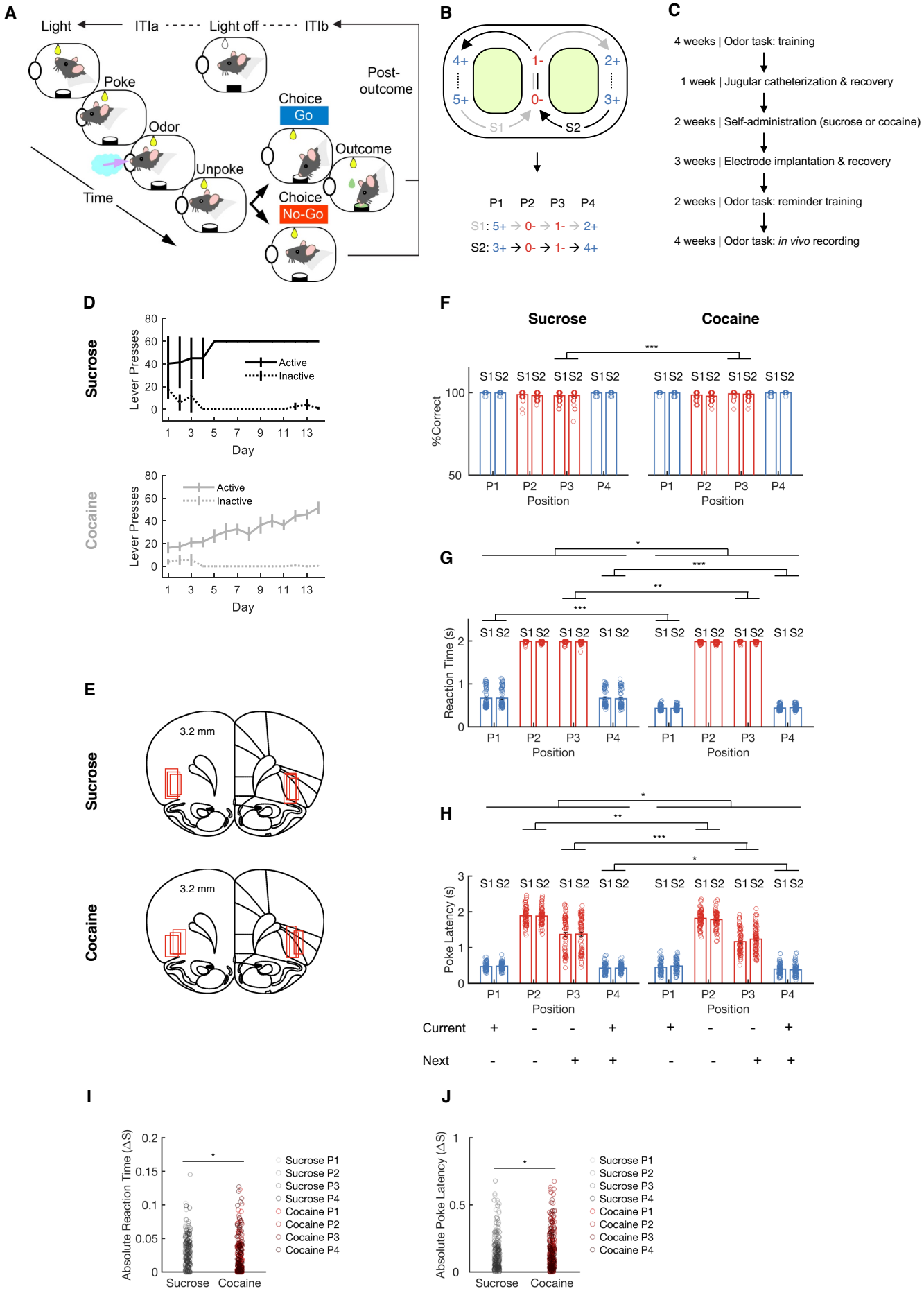

Figure 1. figure 8 odor sequence task and cocaine self-administration

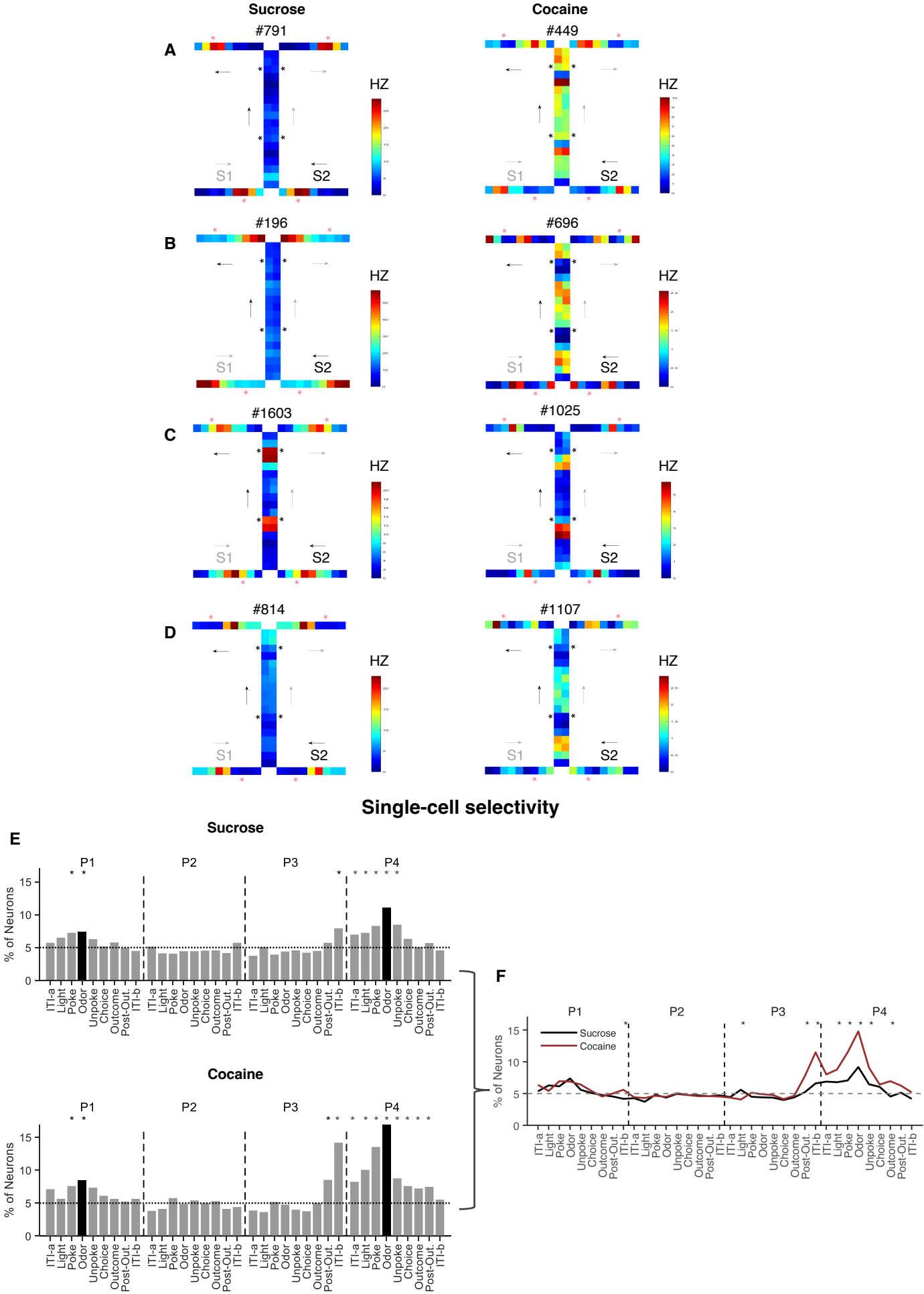

Figure 2. Cocaine use enhances the OFC's ability to discriminate between sequences S1 and S2 at single-cell level

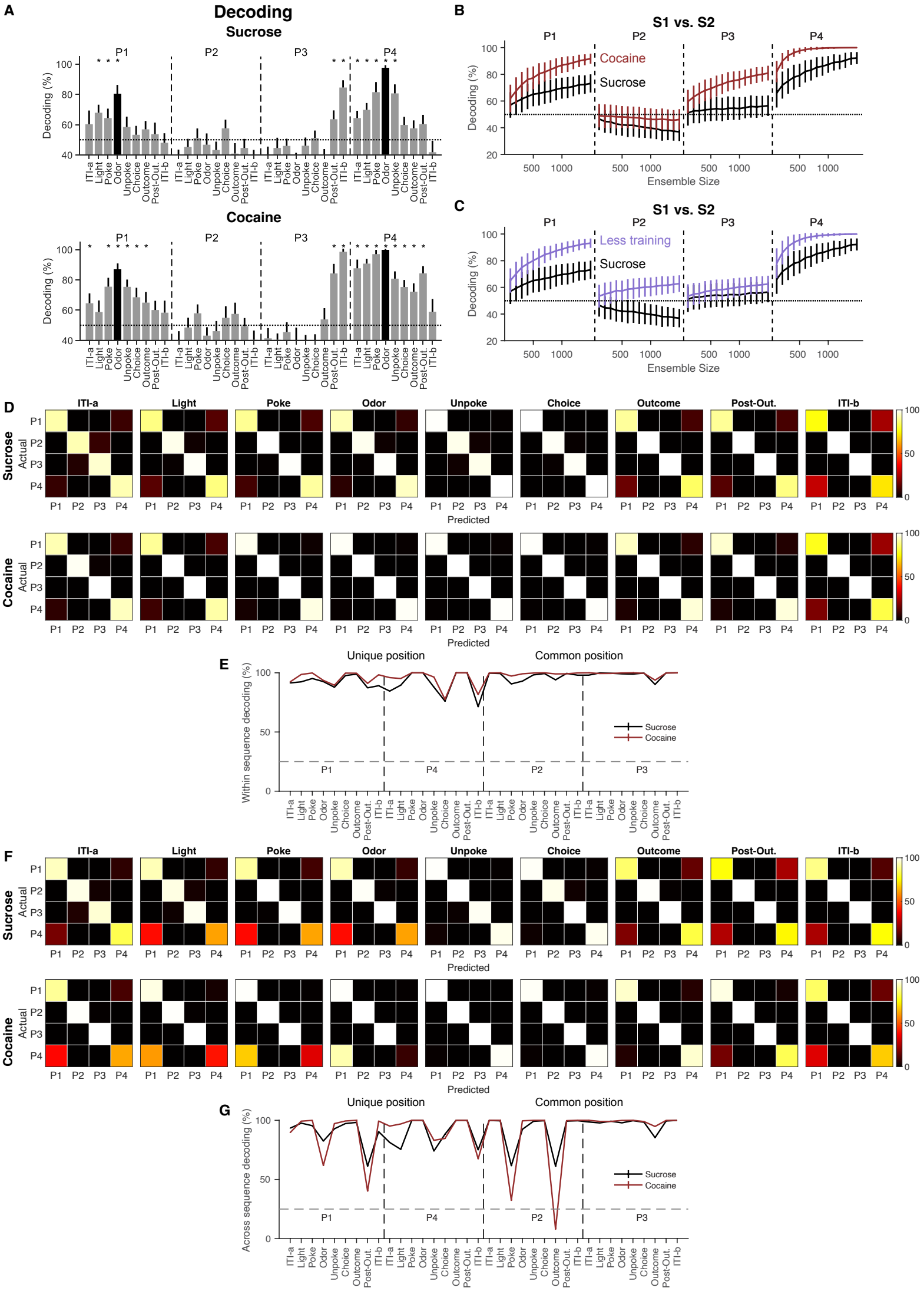

Figure 3. Cocaine use reduces the ability of OFC to generalize task-irrelevant odor-overlapping sequences

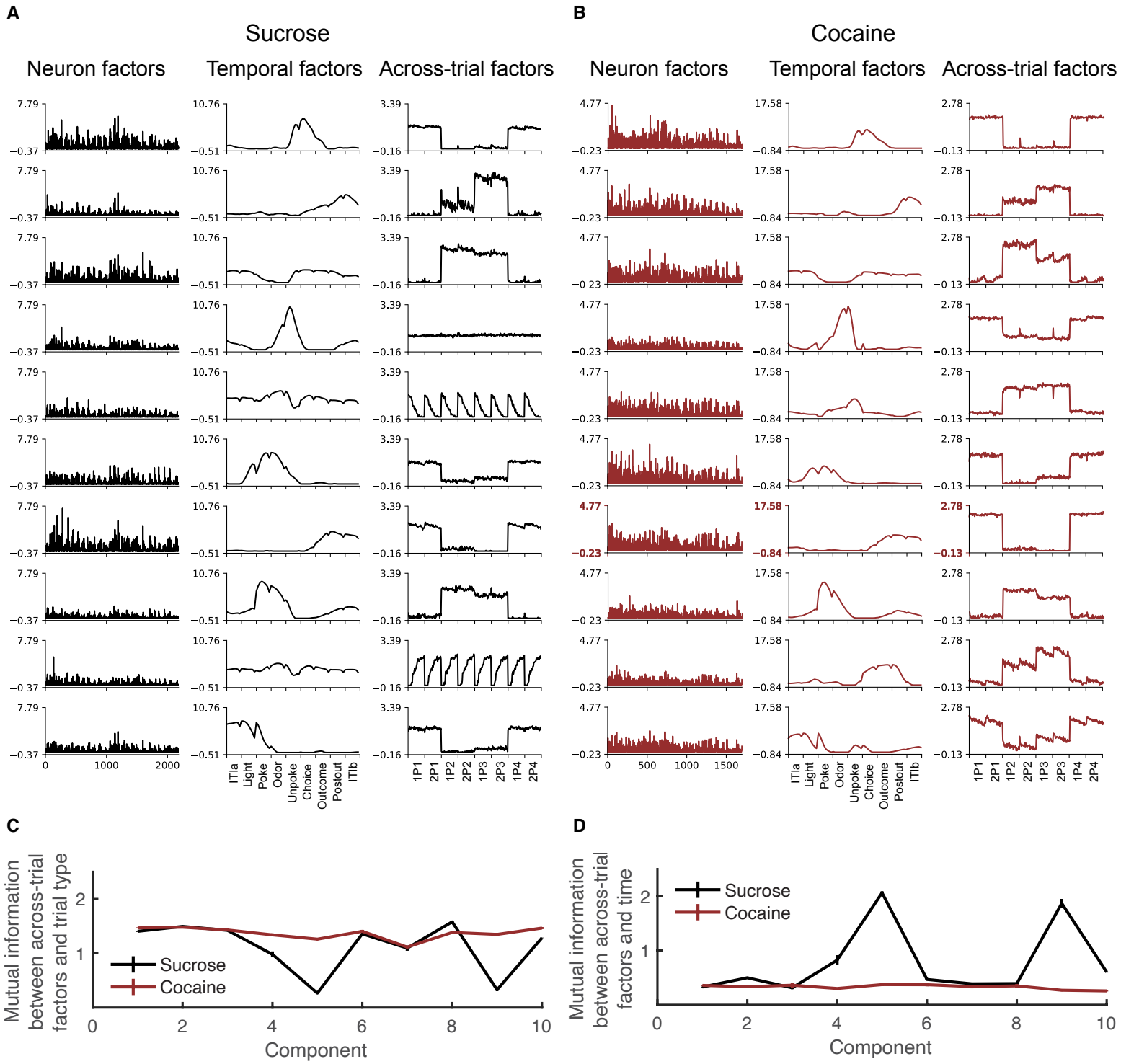

Figure 4. Cocaine use impairs the OFC's function in temporal cognition and decreases the generalization of task-irrelevant odor-overlapping sequences

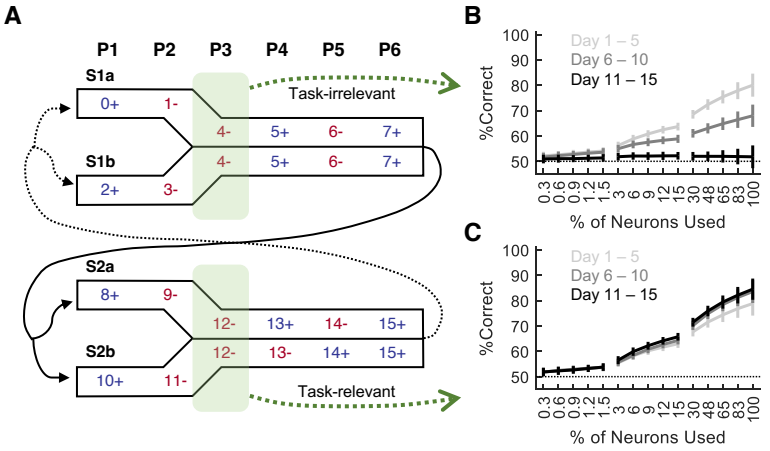

Figure 3—figure supplement 1. The ability of the OFC to generalize task-irrelevant odor-overlapping sequences decreases as learning progresses

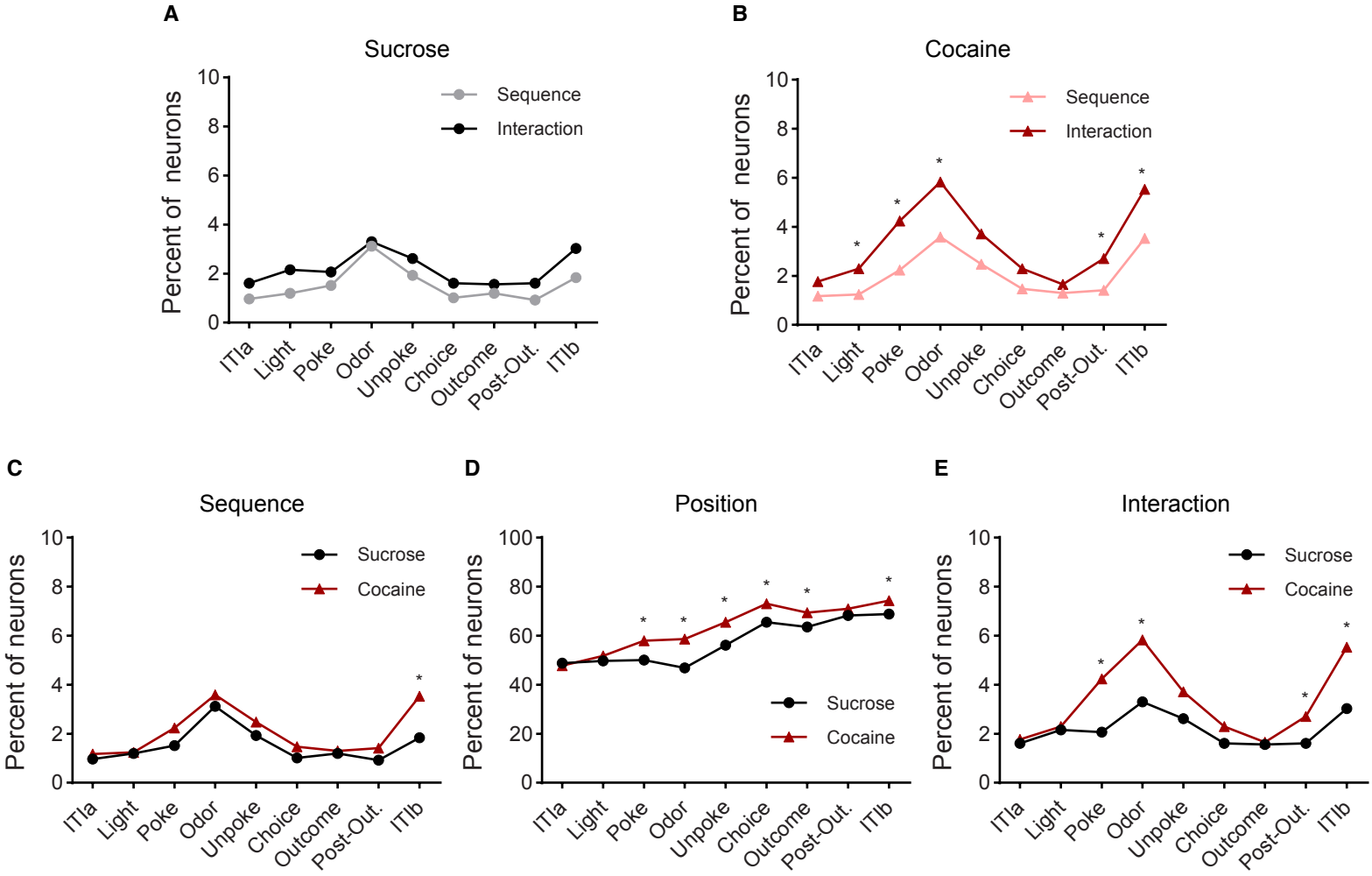

Figure 3—figure supplement 2. Two-way ANOVA of sequence and position effects

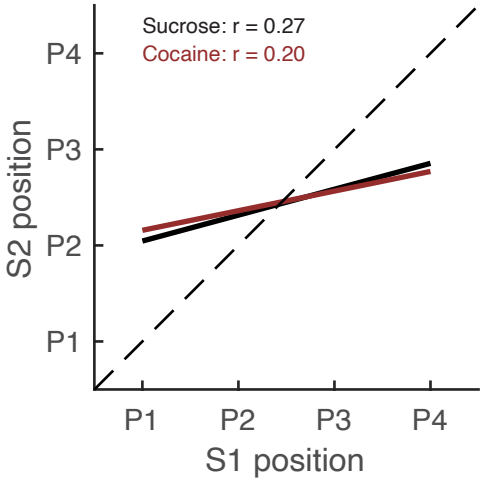

Figure 3—figure supplement 3. Correlation of preferred positions

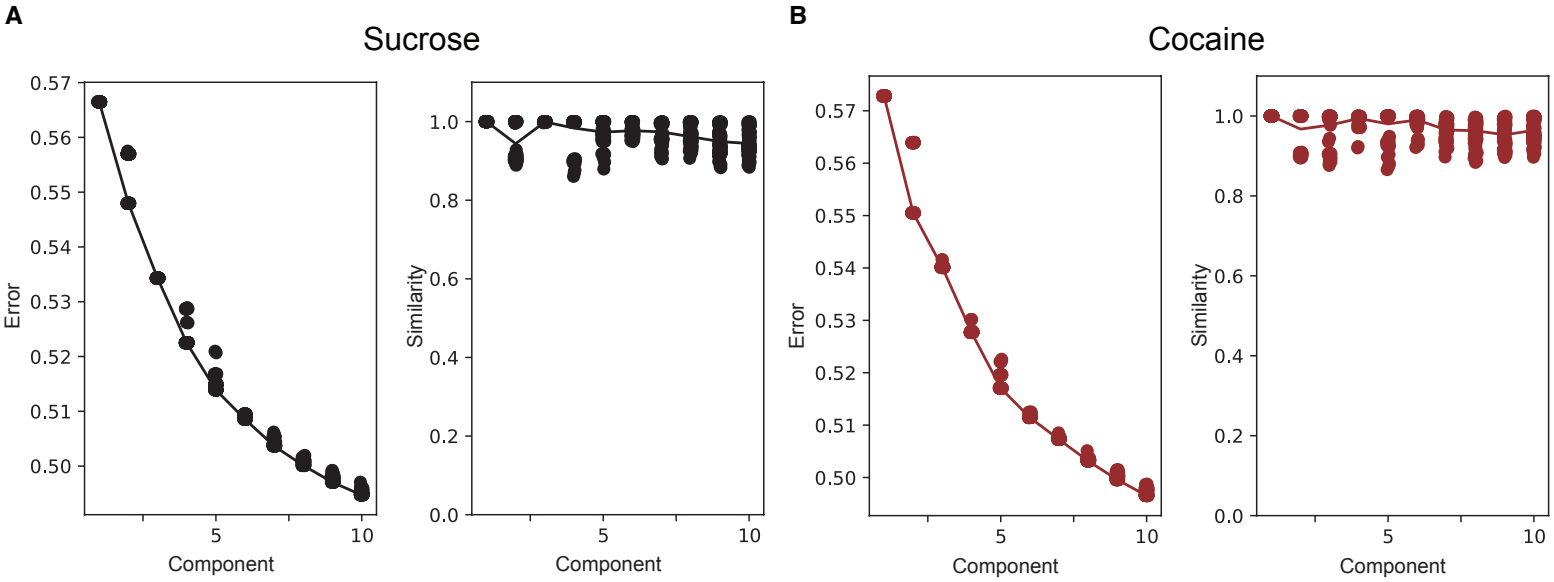

Figure 4—figure supplement 1. Error and similarity plots for TCA

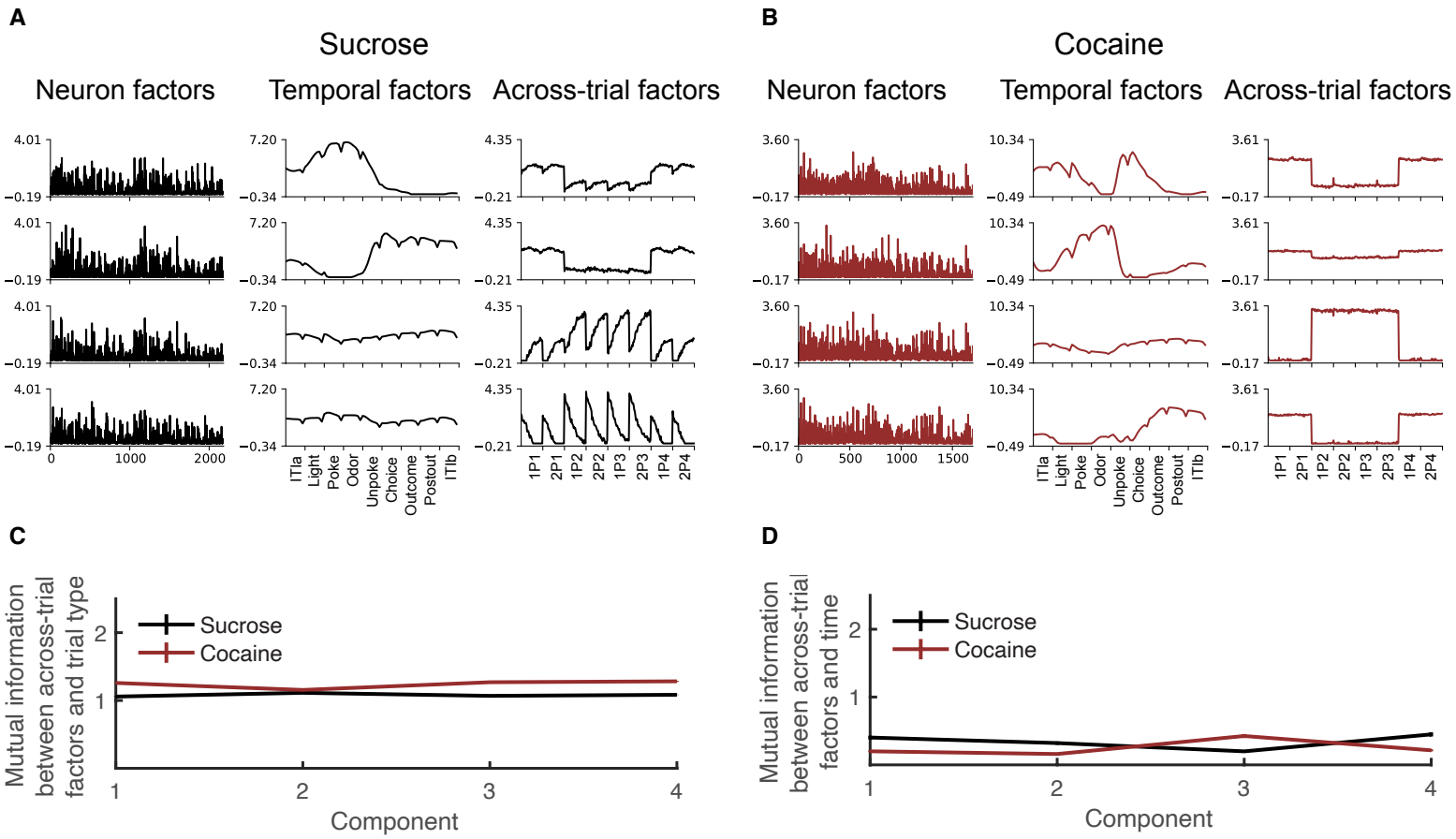

Figure 4—figure supplement 2. Four component model, cocaine impairs OFC temporal cognition and sequence generalization with irrelevant overlapping odors

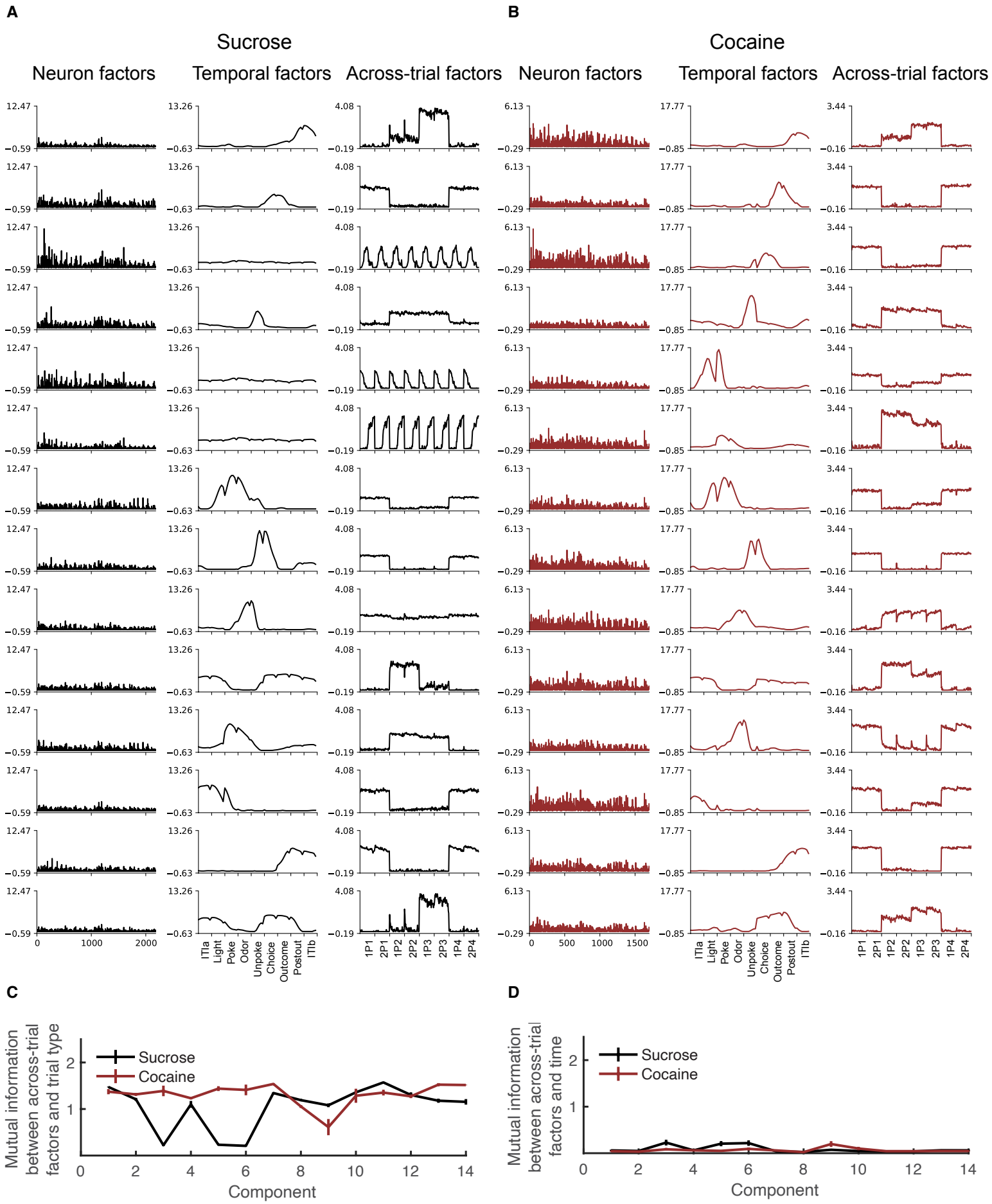

Figure 4—figure supplement 3. Fourteen component model, cocaine use impairs OFC function in temporal cognition and hinders generalization across odor-overlapping, task-irrelevant sequences

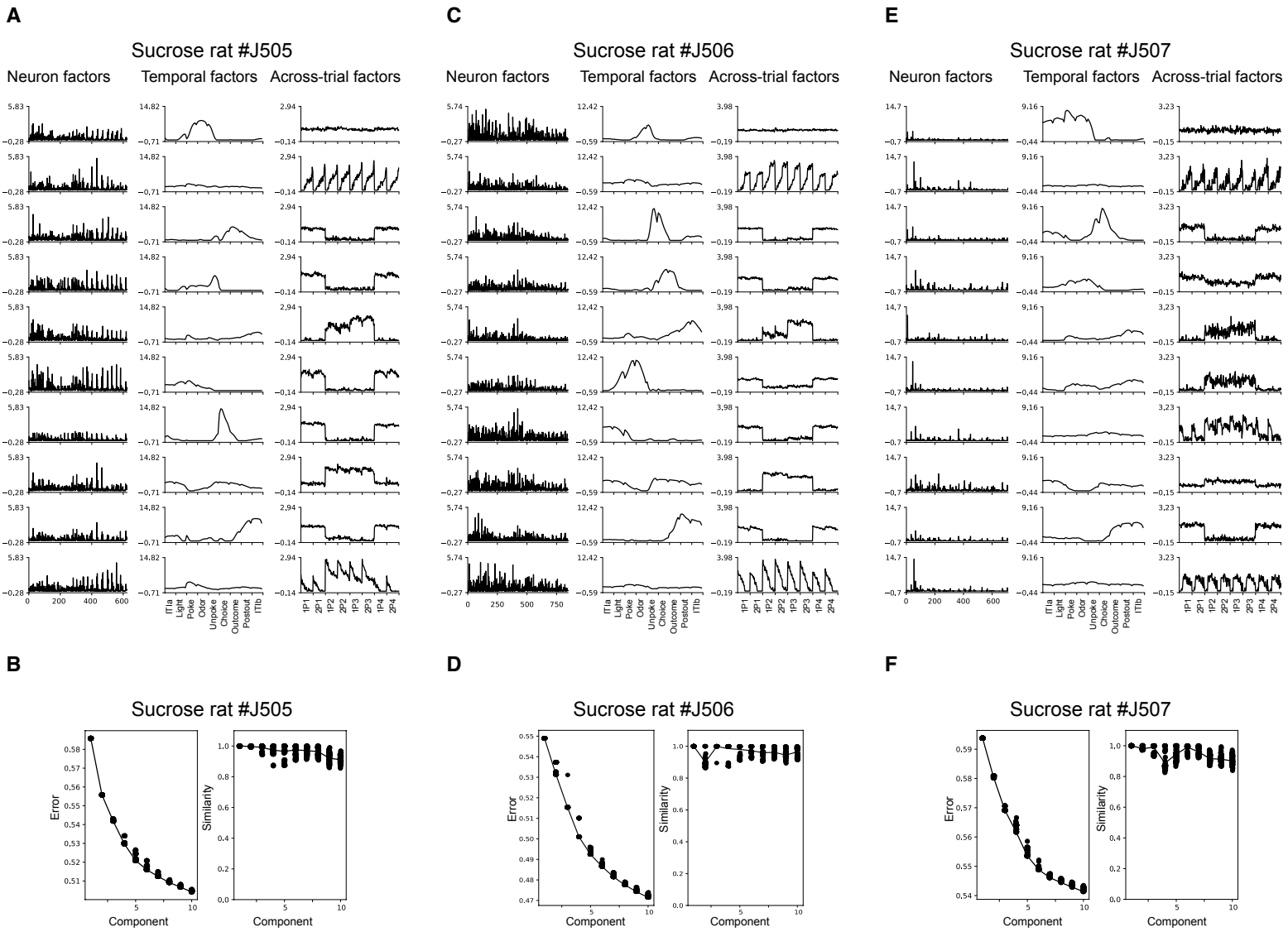

Figure 4—figure supplement 4. Ten-component model for individual Sucrose rats

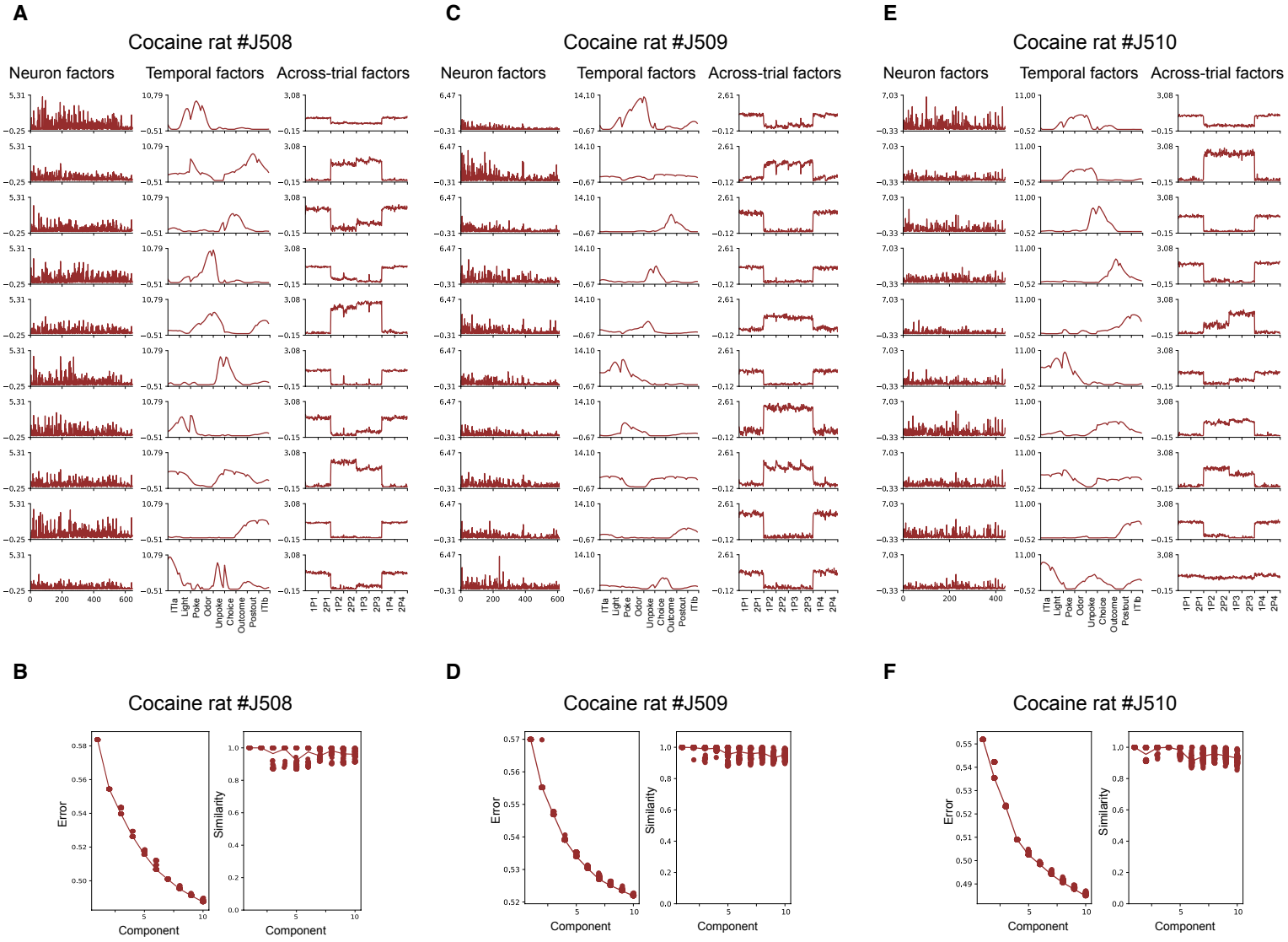

Figure 4—figure supplement 5. Ten-component TCA model applied to individual rats from the Cocaine group